Remote Sensing of Environment 114 (2010) 1325–1337

Contents lists available at ScienceDirect

Remote Sensing of Environment

journal homepage: www.elsevier.com/locate/rse

Estimating aboveground forest biomass from canopy reflectance model inversion in mountainous terrain

Scott A. Soenen [a], Derek R. Peddle [a,*], Ronald J. Hall [b,a], Craig A. Coburn [a], Forrest G. Hall [c,d]

[a] Department of Geography, University of Lethbridge, WESB, 4401 University Drive West, Lethbridge, AB., Canada T1K 3M4
[b] Natural Resources Canada, Canadian Forest Service, 5320–122 Street, Edmonton, AB., Canada T6H 3S5
[c] NASA Goddard Space Flight Centre, Code 614.4, 8800 Greenbelt Road, Greenbelt MD 20771, USA
[d] University of Maryland, Baltimore County, Joint Center for Earth Systems Technology (JCET), USA

ARTICLE INFO

Article history:
Received 1 September 2009
Received in revised form 27 October 2009
Accepted 19 December 2009

Keywords:
Biomass
Canopy reflectance model
Inversion
Forest structure
Carbon
Mountains
Spectral mixture analysis
NDVI

ABSTRACT

The amount and spatial distribution of aboveground forest biomass (AGB) are required inputs to forest carbon budgets and ecosystem productivity models. Satellite remote sensing offers distinct advantages for large area and multi-temporal applications, however, conventional empirical methods for estimating forest canopy structure and AGB can be difficult in areas of high relief and variable terrain. This paper introduces a new method for obtaining AGB from forest structure estimates using a physically-based canopy reflectance (CR) model inversion approach. A geometric-optical CR model was run in multiple forward mode (MFM) using SPOT-5 imagery to derive forest structure and biomass at Kananaskis, Alberta in the Canadian Rocky Mountains. The approach first estimates tree crown dimensions and stem density for satellite image pixels which are then related to tree biomass and AGB using a crown spheroid surface area approach. MFM estimates of AGB were evaluated for 36 deciduous (trembling aspen) and conifer (lodgepole pine) field validation sites and compared against spectral mixture analysis (SMA) and normalised difference vegetation index (NDVI) biomass predictions from atmospherically and topographically corrected (SCS+C) imagery. MFM provided the lowest error for all validation plots of 31.7 tonnes/hectare (t/ha) versus SMA (32.6 t/ha error) and NDVI (34.7 t/ha) as well as for conifer plots (MFM: 23.0 t/ha; SMA 27.9 t/ha; NDVI 29.7 t/ha) but had higher error than SMA and NDVI for deciduous plots (by 4.5 t/ha and 2.1 t/ha, respectively). The MFM approach was considerably more stable over the full range of biomass values (67 to 243 t/ha) measured in the field. Field plots with biomass >1 standard deviation from the field mean (over 30% of plots) had biomass estimation errors of 37.9 t/ha using MFM compared with 65.5 t/ha and 67.5 t/ha error from SMA and NDVI, respectively. In addition to providing more accurate overall results and greater stability over the range of biomass values, the MFM approach also provides a suite of other biophysical structural outputs such as density, crown dimensions, LAI, height and sub-pixel scale fractions. Its explicit physical-basis and minimal ground data requirements are also more appropriate for larger area, multi-scene, multi-date applications with variable scene geometry and in high relief terrain. MFM thus warrants consideration for applications in mountainous and other, less complex terrain for purposes such as forest inventory updates, ecological modeling and terrestrial biomass and carbon monitoring studies.

1. Introduction

Information about forest stand structure and aboveground biomass (AGB) is used to assess forest ecosystem productivity, determine carbon (C) budgets, and support studies of the role of forests in the global carbon cycle (Cihlar et al., 2002; Kurz & Apps, 1999; Lu, 2006; Palacios-Orueta et al., 2005; Zheng et al., 2004). Currently, the most established and frequently used methods for estimating AGB are through the use of field plots or spatial inventory data with statistical or allometric models (Brown, 2002; Fournier et al., 2003; Parresol, 1999). These conventional methods are difficult to extend over large areas because they are limited to where inventory data are available, are spatially incomplete and typically sparse, involve significant time, labour and field costs, and these methods may not be suited for future C reporting since the assessment is often done at one time only (Brown, 2002; Hall et al., 2006). Alternatively, the information content of satellite remote sensing methods are potentially well suited for providing efficient and timely estimates of forest structure and AGB due to the ability to provide both archived and new

* Corresponding author. Department of Geography, University of Lethbridge, Water and Environmental Science Building, 4401 University Drive West, Lethbridge, Alberta, Canada T1K 3M4. Tel.: +1 403 329 2524; fax: +1 403 332 4039.
E-mail address: derek.peddle@uleth.ca (D.R. Peddle).
URL: http://people.uleth.ca/~derek.peddle (D.R. Peddle).

0034-4257/$ – see front matter © 2009 Published by Elsevier Inc.
doi:10.1016/j.rse.2009.12.012

systematic, repetitive, comprehensive observations at local to global scales (Patenaude et al., 2005) as well as being amenable to providing other important related information such as landcover, land-use and photosynthetic functioning at various scales (Cohen et al., 2001; Treitz & Rogan, 2004; Thomas et al., 2006).

While a number of remote sensing techniques for estimating stand structure and AGB have been reported (Coops et al., 2004; De Jong et al., 2003; Fournier et al., 2003; Jensen & Hodgson, 1985; Luther et al., 2005; Labrecque et al., 2005; Leboeuf et al., 2005; Roy & Ravan, 1996; Thenkabail et al., 2004), the variability in results suggests it remains a difficult, challenging task (Hyyppä et al., 2000; Foody et al., 2003; Lu, 2006; Rosenqvist et al., 2003). Statistical techniques are among those most frequently used, whereby multispectral satellite data or derived values (e.g. vegetation indices, mixture fractions) are empirically related to stand structure and biomass (Gerylo et al., 2002; Hall et al., 2006; Wulder, 1998). Some success has been reported in applications of these methods in areas of limited terrain relief (Gerylo et al., 2002; Hall et al., 2006; Hame et al., 1997; Franklin et al., 2003; Peddle, Brunke, et al., 2001). The relationships between satellite data and stand characteristics, however, can be adversely influenced in areas of high topographic variation (Gemmell, 1995, 1998), or in areas where surface features such as exposed rock and soil can lead to mixed pixels that can further confound the relationship with biomass (Elvidge & Lyon, 1985).

An alternative to statistical methods is the inversion of canopy reflectance models (Leblanc & Chen, 2000; Scarth & Phinn, 2000). Geometric-optical canopy reflectance models in particular provide a direct physical characterisation of the relationship between forest stand structure, terrain geometry, view angle, illumination angle, surface properties, and the radiometric response from satellite data (Chen et al., 2000; Hall et al., 1997). Inversion of these models to provide information about forest stand structure has shown promising results (Wu & Strahler, 1994; Woodcock et al., 1997), however, the inversion procedure can be computationally intense and thus inappropriate for large study areas and time sensitive accounting. Further, some of these models are either non-invertible or yield non-exact or no solutions. To overcome these problems and increase the efficiency of canopy reflectance model inversion, it is necessary to use indirect inversion methods where canopy reflectance is pre-computed (Kimes et al., 2000). These look-up table (LUT) methods were subsequently used successfully in agriculture (Weiss et al., 2000), forestry (Peddle, Franklin, et al., 2003) and a variety of follow-on studies (Peddle, Franklin, et al., 2003; Peddle, Luther, et al., 2003; Peddle et al., 2004, 2007; Peddle, Boon, et al., in press; Peddle, Huemmrich, et al., in press; Soenen et al., 2005, 2008, 2009) involving first-order biophysical parameters, but has not been extended past the primary parameter set to obtain second-order biophysical parameters such as AGB.

This paper introduces a new method for estimating AGB from satellite imagery over mountainous terrain using canopy reflectance models that explicitly characterize the variation in reflectance due to different vegetation properties, topography, illumination (solar) and view (sensor) angles. This approach first estimates average tree crown dimensions and stem density for a satellite image pixel through indirect inversion of a geometric-optical canopy reflectance model, then relates the crown dimensions and stem density to average tree biomass and AGB for the pixel. Accordingly, the objectives of this study were:

(i) Describe this two-step canopy reflectance model based approach;
(ii) Evaluate results against AGB field validation data collected in a mountainous study area; and
(iii) Compare results from the canopy reflectance model approach to other multispectral image-based approaches including spectral mixture analysis and vegetation indices (Peddle, Brunke, et al., 2001).

The canopy reflectance model approach was hypothesized to generate more accurate estimates of AGB than those from empirical multispectral image-based approaches on the basis that (i) the explicit physically-based context provided by canopy models is theoretically more appropriate, (ii) the approach has been demonstrated as superior to other methods in past studies (Peddle, Franklin, et al., 2003) and a variety of follow-on studies (Peddle, Franklin, et al., 2003; Peddle, Luther, et al., 2003; Peddle et al., 2004, 2007; Peddle, Boon, et al., in press; Peddle, Huemmrich, et al., in press; Soenen et al., 2005, 2008, 2009) involving other biophysical structural estimates, and (iii) it encompasses an explicit terrain handling module that utilizes terrain geometry information to advantage, instead of avoiding or trying to correct for it as in most other studies.

2. Methods

2.1. Study area

The study area (Fig. 1) was centered at 51.02° N, 115.07° W in the northern part of Kananaskis Country Provincial Park, Alberta, Canada. The area encompassed 180 km^2 of terrain in the east slopes of the Front Range of the Canadian Rocky Mountains with terrain elevations ranging from 1400 m to 2100 m above sea level, and slopes ranging from 0° to 55° over a full range of terrain aspect. The study area included both Montane and Sub-Alpine vegetation zones (Archibald et al., 1996). The dominant overstory coniferous species was lodgepole pine (*Pinus contorta* var. *latifolia* Dougl ex. Loud.), as well as white spruce (*Picea glauca* (Moench) Voss), Engelmann spruce (*Picea engelmannii* Parry ex Engelm.), Douglas-fir (*Pseudotsuga menziesii* (Mirb.) Franco), and sub-alpine fir (*Abies lasiocarpa* (Hook) Nutl.). The dominant deciduous tree species was trembling aspen (*Populus tremuloides* Michx.), and balsam poplar (*Populus balsamifera* L.), with lesser amounts of white birch (*Betula papyrifera* Marsh.). Stand age within the study area was typically between 90 to 120 years for conifer stands and 50 to 90 years for deciduous stands.

2.2. Image and terrain data

Système pour l'Observation de la Terre (SPOT) satellite imagery covering the study area were acquired August 12, 2004 by the High Geometric Resolution (HGR; SPOT 5) sensor at a −7.3° off-nadir view angle. The cloud-free, 10 m multispectral SPOT data were resampled to 25 m to match the resolution of an associated digital elevation model (DEM) and orthorectified to within sub-pixel scale (<5 m) positional error based on an independent ground control point based assessment.

Atmospheric correction of the SPOT imagery involved several steps. First, the image data were converted from raw digital numbers (DN) to at-sensor radiance using published calibration gain and offset values available from SPOT Image Corporation (SPOT Image, 2004). Each image band was then calibrated to top of the atmosphere reflectance based on the earth–sun distance at the time of image acquisition and the solar irradiance for a given band from SPOT Image (2004). A further calibration procedure to account for atmospheric transmission and path radiance was applied to the SPOT data using field spectral measurements of pseudo-invariant features obtained near the time of image acquisition (Milton et al., 1997; Schott et al., 1988). The SPOT data were then transformed using the empirical line method (Smith & Milton, 1999) to complete this part of the atmospheric correction.

Topographic correction of the SPOT image data was achieved using the SCS+C method implemented by Soenen et al. (2005) as a modification of the sub-pixel scale Sun-Canopy-Sensor (SCS) method of Gu and Gillespie (1998). The SCS framework introduced by Gu and Gillespie (1998) was a significant advance in topographic correction as it preserves the geotropic nature of vertical tree growth

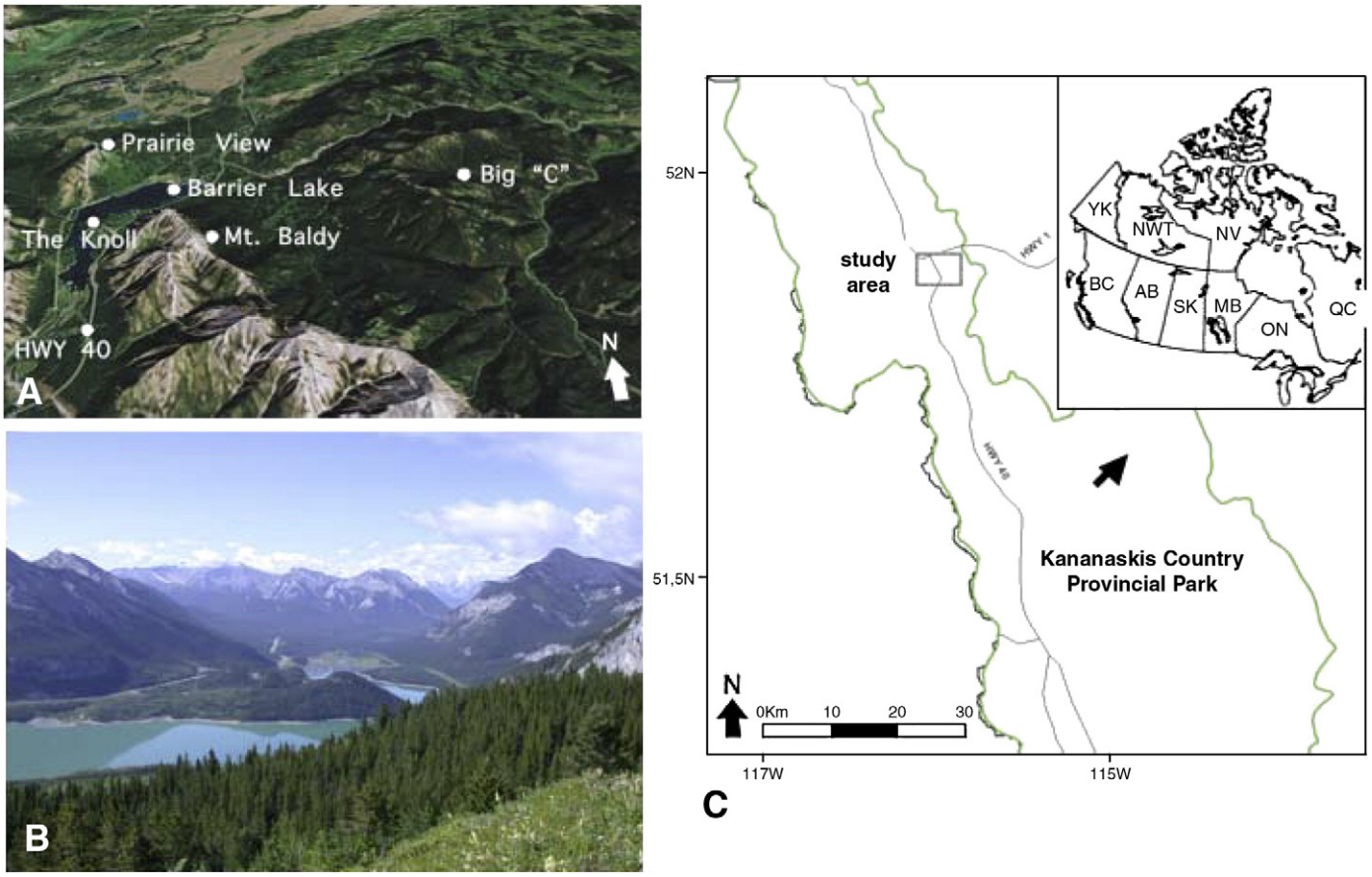

Fig. 1. Study area, Canadian Rocky Mountains: A): natural colour satellite image showing field areas and access road; B) looking south from Prairie View across Barrier Lake; northern flank of Mount Baldy to left; C) general study area location in Kananaskis, Alberta, in western Canada.

regardless of terrain, view and illumination angles, and is therefore preferable to traditional photometric Sun-Terrain-Sensor (STS) methods that violate this fundamental physical relationship. The SCS+C topographic correction of Soenen et al. (2005) further modified the SCS approach to account for diffuse atmospheric irradiance based on an additional C-correction that compensates for the overcorrection at higher incidence angles experienced by SCS. The Kananaskis study area in this paper was extensively investigated in terms of topographic correction by Soenen et al. (2005) in which it was found SCS+C was superior to SCS and the photometric STS topographic corrections (cosine, Minnaert statistical–empirical, C-Correction). In this work, the SCS+C topographically corrected image data were subsequently used to derive NDVI values and SMA fractions. However, the SCS+C-correction was not required for MFM since topography is already included directly in the canopy reflectance model used with MFM in this study, as described in detail in Soenen et al. (2008) which investigated topographic correction of the SPOT image data set used here. Since terrain slope and aspect were incorporated directly in the modeling of forest structure in MFM, topography was handled internally and no additional external topographic correction was required. Accordingly, the internal MFM-based topographic correction capability is included as one aspect of the overall comparison with the other methods.

2.3. Field data

Field data from 36 field plots were collected during two consecutive field seasons (2003 and 2004). Twenty one field plots were located within conifer dominant (>80% stem count) stands and 15 plots were located within deciduous dominant stands. Plot size was set at 0.04 ha (400 m^2) to ensure that at least one 10 m image pixel would spatially coincide with each plot (i.e. image data were associated with field plots based on individual pixels). To ensure an adequate representation of the range of terrain and stand density conditions within the study area, a stratified sampling protocol was used with field plot locations derived randomly within DEM derivative classes and forest classes from the Alberta Vegetation Inventory (AVI, 1991). AGB validation data were calculated for each plot from field measurements of diameter at breast height (dbh) and tree heights. Other data, including crown dimensions and vegetation spectral response, were recorded for canopy reflectance model parameterization and to validate initial inversion results.

Measurements of total tree height, height to crown center (HTC), dbh, horizontal and vertical crown radius were taken for each tree within a field plot. In addition, species data and stem counts for each plot were recorded. Tree heights and height to crown center were measured using a digital clinometer at 20 m distance. Vertical crown radius was determined by subtracting the height to the base of the canopy (a parameter easily and accurately measured) from the total height, and dividing in half. The horizontal crown radius for each tree was measured using a GRS densiometer to determine the vertical projection of the edges of the crown to the ground (i.e. the drip-line). The distance from the drip-line to the trunk was then measured. This process was repeated perpendicular to the first measurement to characterize variation in horizontal crown dimensions.

Endmember spectral measurements were acquired in the field for input to the SMA and MFM procedures. Three endmembers were used for each tree species: sunlit canopy, sunlit background, and shadow, consistent with previous MFM and SMA studies in this area using satellite and airborne imagery, respectively (Peddle & Johnson, 2000;

Soenen et al., 2008) as these are the primary image components that drive pixel level reflectance in this area. Reference (field) spectra were required because the spatial resolution of the satellite imagery was insufficient to use image pixels as endmember values. Using an Analytical Spectral Devices (ASD) Field-Spec spectroradiometer (ASD, 1998), the spectral properties of sunlit and shadowed vegetation were measured throughout 350–2500 nm using optically thick stacks of Trembling Aspen and Lodgepole Pine samples and used for the sunlit canopy and shadow endmember for each species, with the sunlit background endmember spectra acquired for understory vegetation compositions observed in the field plots, following the protocols established and tested in Peddle and Johnson (2000). The measurements occurred near the expected satellite overpass time on cloud-free dates in June and July, 2004. All spectral measurements were processed to reflectance with respect to calibrated white reference panel readings following protocols by Peddle, White, et al. (2001) and used the same surface orientation as the topographically corrected imagery. To ensure a high signal to noise ratio, the spectroradiometer was configured to acquire 10 measurements per unit interval which were then averaged for each sample. Dark current calibrations and white reference measurements were completed prior to each target measurement to account for any internal signal noise and illumination variations during measurement. The field spectra were subsequently processed to correspond to the specific SPOT image wavelength bands based on published spectral response functions for each satellite sensor band (SPOT Image, 2004).

2.4. Estimating tree biomass from field data

Destructive sampling was not permitted in the Kananaskis study area to measure tree biomass (B). Instead, aboveground total individual tree biomass was calculated for each tree within plot boundaries using dbh within the log-transformed power model and regression coefficients (Table 1) from Case and Hall (2008):

$$\ln(B) = b_0 + b_1 \ln(dbh). \quad (1)$$

It was necessary to apply a correction factor (Table 1) to account for the skewness in the distribution in arithmetic units when converting from the logarithm of tree biomass to original biomass units (Baskerville, 1972). The B (tonnes·tree^{-1}) was then summed for each plot and divided by the plot area to give total biomass (tonnes) within the plot and total standing AGB (tonnes ha^{-1}).

2.5. Multiple forward mode retrieval of canopy structural parameters

The SPOT image data were linked to forest canopy structural conditions through the multiple forward mode (MFM) canopy reflectance model inversion method using the Li and Strahler (1992) geometric-optical mutual shadowing (GOMS) canopy reflectance model. The MFM method is an indirect, look-up table based approach to canopy reflectance model inversion that consists of a set of algorithms for LUT creation (Kimes et al., 2000; Peddle, Franklin, et al., 2003) and LUT search and description of potential inversion solutions (Soenen et al., 2009). MFM has been applied successfully in a variety of applications and locations using different sensors and models (Peddle, Franklin, et al., 2003; Peddle, Luther, et al., 2003; Peddle et al., 2004, 2007; Peddle, Boon, et al., in press; Peddle, Huemmrich, et al., in press; Soenen et al., 2005, 2008, 2009) with broader perspectives on MFM provided in Cihlar et al. (2003) and Gamon et al. (2004). A detailed description of the MFM method has been provided by Peddle et al. (2004, 2007) and Soenen et al. (2009) and is not repeated here. Instead, a brief description of MFM with a focus on its use within the experimental design (Fig. 2) for deriving AGB in this study is provided.

In the first MFM stage (Fig. 2), LUTs were created for each image band from a set of model input canopy structure parameters and the corresponding modeled reflectance output. Range and increment size were selected for each model input parameter from which the parameter sets were generated for the iterative model runs (Table 2). Two input parameter sets were used for each species: 1) a general range of structure covering the full range of potential canopy conditions in the area; and 2) a refined range of structure bounded by two standard deviations from the mean of the observed field structure conditions. The first parameter set simulated limited knowledge of field conditions, and the second parameter set was used to determine if improvements in prediction accuracy could be obtained with a refined parameter set. Each set of inputs was tested separately using the standard MFM one-step approach, different than the two (or more) step optimization procedures implemented in Peddle, Boon, et al. (in press) for situations of reduced or no input ground data. Each entry in the LUT was created through a forward mode execution of the GOMS model using the structural parameter sets as input. The resulting LUTs contained all possible structural input parameter combinations and the output (forward mode) modeled GOMS reflectance values used for matching with each satellite image band, as well as the computed scene fractions (not used in this study). The LUT also contained all associated forest structure, terrain geometry and illumination and view angles as well as spectral parameters used to generate each forward mode reflectance output.

Structural parameters were retrieved in the second MFM stage (Fig. 2). The MFM LUT algorithm searches the LUT for modeled reflectance values that were within a predefined spectral range from the image reflectance from all SPOT image bands for each pixel. The spectral range was defined using the relative root mean square error (RMSE) between measured (ρ_i) and modeled (ρ_m) reflectance for the number of image bands (n_b) (Weiss et al., 2000; Soenen et al., 2009):

$$RMSE = \sqrt{\frac{1}{n_b}\sum_{i=1}^{n_b}\left(\frac{\rho_i - \rho_m}{\rho_i}\right)^2}. \quad (2)$$

The structural parameters in the LUT associated with the matching modeled reflectance values within the spectral range were then selected as potential inversion results. The distribution of potential inversion results contained the following structural parameters of interest: stem density (d), horizontal crown radius (r), vertical crown radius (b) and species.

2.6. Estimating tree biomass from a crown spheroid area based empirical model

A regression model was created to relate r and b parameters, summarized as crown surface area (SA), to tree biomass for stands of a uniform age (Fig. 2). The r and b parameters were selected for the biomass model over height to crown because they can be more accurately predicted due to their influence on the relative proportions of the primary drivers of pixel level reflectance: sunlit and shadowed canopy and ground area. Crown SA was related to biomass as an analogue to the area of the crown supporting physiological processes. Surface area was calculated using maximum horizontal and vertical crown radial extent within spheroid area equations consistent with

Table 1
Tree level regression coefficients, statistics and correction factor (C.F.) from Case and Hall (2008) used in the estimation of tree biomass from field data.

Species	b_0	b_1	r^2	RMSE	C.F.
Lodgepole pine	−2.021	2.274	0.94	25.2	1.019
Trembling aspen	−2.763	2.524	0.94	39.7	1.022

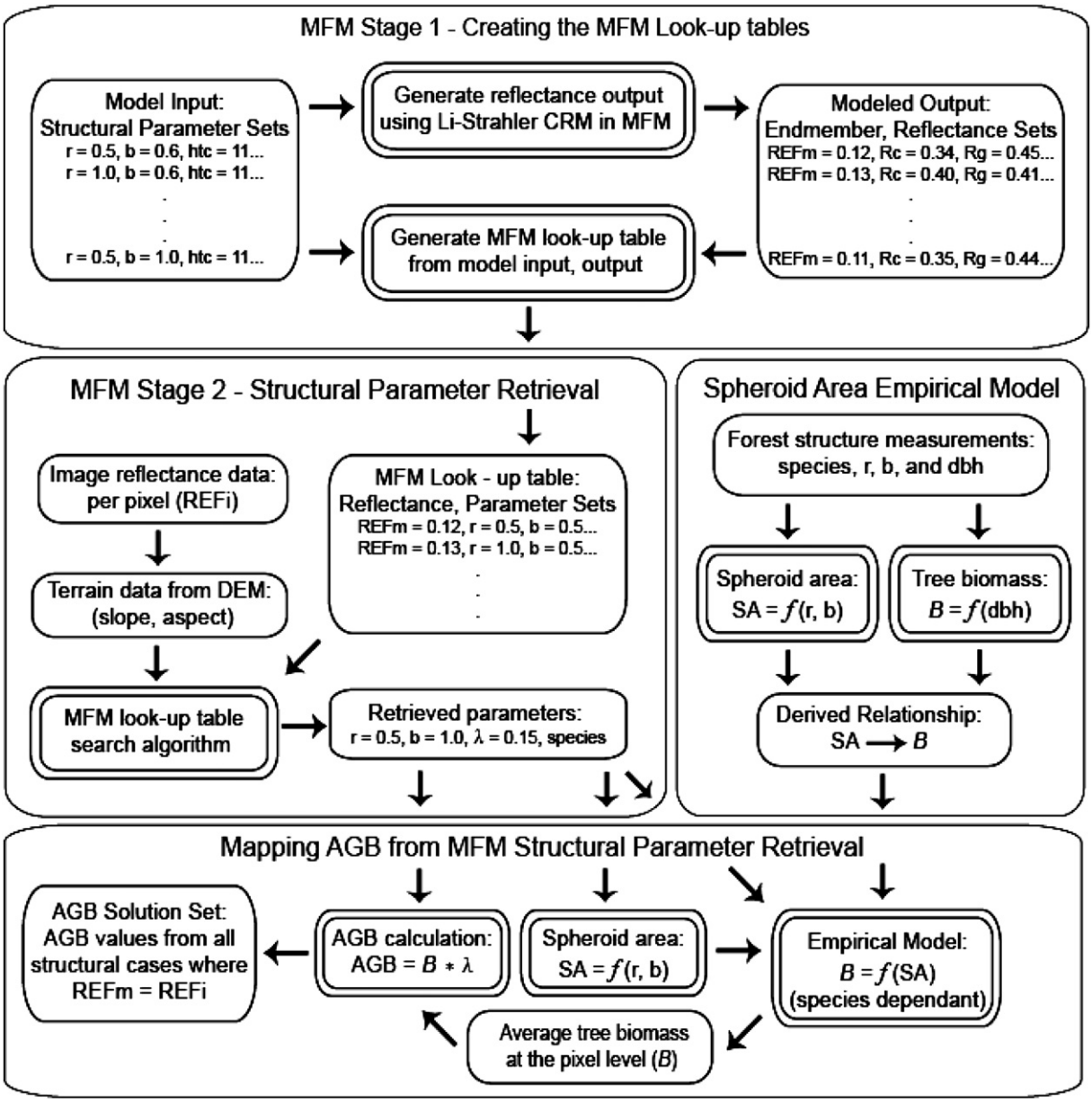

Fig. 2. Flowchart of methods for MFM estimation of AGB.

Table 2
MFM structural and terrain inputs used in creating a general set of LUTS based on a full range of structural inputs with coarser increments, and a refined set of LUTs (input range: ±2 standard deviations of field mean) with finer increments. Parameter set sizes corresponding to number of LUT entries shown for each species and LUT type.

	Structural parameter	General			Refined		
		Min	Max	inc	Min	Max	inc
Lodgepole pine	Density – λ (trees/m^2)	0.05	0.5	0.05	0.06	0.26	0.02
	Horizontal crown radius – r (m)	0.5	6.5	1	0.5	2.5	0.5
	Vertical crown radius – b (m)	0.5	6.5	2	1	4	1
	Height to crown center – h (m)	4	14	2	10	14	1
	Height distribution – dh (m)	5	25	5	6	16	2
	Slope – α (°)	0	60	10	0	40	5
	Aspect – φ (°)	0	315	45	0	315	45
	Size of parameter set	529200			445500		
Trembling aspen	Density – λ (trees/m^2)	0.05	0.5	0.05	0.06	0.2	0.02
	Horizontal crown radius – r (m)	0.5	6.5	1	1	4	0.5
	Vertical crown radius – b (m)	0.5	6.5	2	1	3	1
	Height to crown center – h (m)	4	14	2	11	15	1
	Height distribution – dh (m)	5	25	5	6	20	2
	Slope – α (°)	0	60	10	0	20	5
	Aspect – φ (°)	0	315	45	0	315	45
	Size of parameter set	829440			302400		

physical parameters of the GOMS model. Equations used for prolate spheroid area (SA_p) and oblate spheroids (SA_o) were:

$$SA_p = \pi\left(2r^2 + \frac{b^2}{e}\ln\left(\frac{1+e}{1-e}\right)\right) \quad (3)$$

and

$$SA_o = 2\pi b\left(b + r\frac{e^{\frac{1}{\sin}}}{e}\right) \quad (4)$$

where e is the ellipticity or eccentricity defined as:

$$e_p = \sqrt{1-\frac{r^2}{b^2}} \quad (5)$$

$$e_o = \sqrt{1-\frac{b^2}{r^2}}. \quad (6)$$

The new SA-based tree biomass allometric equation was created for both conifer and deciduous trees using linear least squares regression. Regression models were generated using a dataset consisting of field measurements of crown dimensions (r, b) and previous calculations of tree biomass from the dbh-based log-transformed power model for 350 individual trees from each species type.

2.7. Mapping AGB from MFM structural parameter retrieval

After calculating SA from the estimates of r and b in each set within the distribution of retrieved structural parameters from the second stage MFM estimates of crown dimension, the SA-based allometric equations were applied to predict average tree biomass within the area covered by the image pixel (Fig. 2). Average tree biomass (B) was then aggregated to total aboveground biomass for all trees within the area covered by the pixel by multiplying the estimate of d, in units of trees per unit area, by the average tree biomass ($AGB = B \cdot d$). The result was a set of solutions for potential AGB of the pixel area. The values written to the output AGB map were summarized from the solution set using the median value that was shown to be the most suitable statistic for solution distributions (Weiss et al., 2000).

2.8. AGB estimation using NDVI and spectral mixture analysis

For comparative purposes, biomass density was also estimated using empirical relationships with the normalised difference vegetation index (NDVI) and the sub-pixel scale shadow fraction from spectral mixture analysis (SMA). These two multispectral image approaches have been used extensively in past studies in flat and low relief terrain (e.g. Lu et al., 2005; Peddle et al., 1999; Peddle, Brunke, et al., 2001; Zheng et al., 2004) and thus were deemed as appropriate methods for comparison with MFM, particularly owing to the extensive set of topographic corrections that had been tested in previous studies for this study area (Soenen et al., 2005, 2008) that provided excellent inputs to NDVI and SMA. It was also deemed important to compare MFM with methods that are familiar and have been used elsewhere, to provide both context as well as new insight into their applicability in areas of more complex forest and terrain. Unlike MFM, which is a physically-based approach that derives biomass from forest structural output, the NDVI and SMA approaches estimate biomass by using empirical equations between biomass ground data and corresponding NDVI and SMA pixel values. NDVI (Rouse et al., 1973) was calculated using SPOT bands 2 (red) and 3 (near infrared, NIR) as $(NIR-red) \div (NIR+red)$. Although a large number of other vegetation indices exist (Bannari et al., 1995; Chen, 1996), NDVI was chosen due to its popularity, ease of computation, and due to the functional equivalence of many VI's (Perry & Lautenschlager, 1984; Peddle, Brunke, et al., 2001).

SMA was performed using the ENVI linear unmixing SMA module (ENVI, 2005) with endmember spectra collected in the field to determine the fractions of sub-pixel scale sunlit canopy, background and shadow for the SPOT imagery. Shadow fraction was used for input to the biomass derivations on the basis of scene theory and previous studies (Franklin et al., 1991; Peddle et al., 1999; Peddle, Brunke, et al., 2001; Seed & King, 2003) where it was determined that this was the optimal endmember for predicting forest biophysical structural variables.

AGB was derived separately from each of NDVI and SMA output using a standard cross-tabulation ("leave-one-out") method (Green, 1979; Köhl et al., 2006; van der Heijden et al., 2007). This involved iteratively removing one AGB plot from the full set, fitting a regression equation to the remainder of the plots, and applying the equation to predict AGB for the "left-out" plot. This was repeated for each plot in the sample to produce the set of plot-based biomass estimates from each of NDVI and SMA. If a full biomass map was required, these predictive equations could be aggregated and applied at each pixel in the image. However, as discussed in Section 3.4.4, only the MFM biomass map was produced, therefore, an aggregated regression equation for each of NDVI and SMA was not required.

2.9. AGB validation against field data

The accuracy of each biomass estimation approach (MFM, SMA, and NDVI) was then assessed against the field-derived biomass validation data. Error (difference between estimated and field data) was determined for each approach for all plots. This was also assessed separately for the individual sets of conifer and deciduous plots to provide species-specific AGB validation. To further assess the capability of each approach to estimate the full range of biomass values found throughout the study area, a further analysis was performed in which the field AGB data were separated into the set of field plots that were within one standard deviation (1 SD) of the overall field biomass mean, and those plots that had biomass values that exceeded 1 SD of the overall mean. This was done for each of conifer, deciduous, and the combined sets of plots. In all cases, the results from MFM, SMA and NDVI were compared, and where possible, placed in the context of results obtained from other studies.

3. Results

3.1. Measured forest stand structure and biomass within field plots

Field measurements and field-derived biomass data for lodgepole pine and trembling aspen plots are summarized in Table 3. Aspen trees in the study area were slightly larger than pine, with an average

Table 3
Descriptive statistics for field measured horizontal crown radius (r), vertical crown radius (b), tree height (h), diameter at breast height (dbh), stem density (λ), and AGB measured within lodgepole pine and trembling aspen validation plots.

		r (m)	b (m)	h (m)	dbh (cm)	λ (stems/ha)	Biomass (t/ha)
Lodgepole	Mean	1.0	3.0	15.1	17.3	1500	141
Pine	SD	0.4	1.2	3.3	5.4	600	34
Plots = 21	Minimum	0.2	0.5	4.3	5.0	775	73
Trees = 1221	Maximum	3.1	8.4	24.7	34.8	3025	213
Trembling	Mean	1.6	1.6	14.6	18.8	1200	155
Aspen	SD	0.6	0.8	3.2	5.1	400	46
Plots = 15	Minimum	0.3	0.4	7.9	8.1	725	67
Trees = 667	Maximum	3.4	4.3	22.9	37.2	1850	243

dbh of 18.8 cm and 17.3 cm respectively. Heights were similar between the two species with mean conifer stand height only 0.5 m greater than deciduous stand height. Stem density ranged from 725 stems/ha to 3025 stems/ha, with the majority of plots ranging from 800 to 1600 stems/ha, with higher densities on average occurring within conifer dominant stands. Vertical crown radius ranged from 0.4 to 8.4 m and was typically larger and more variable in conifer stands than in deciduous stands. The range of horizontal crown radius was similar between the two species types, though deciduous stands had a larger r on average. The average conifer stand AGB (141 t/ha) was smaller than deciduous stand AGB (155 t/ha), a result of its larger average basal area (Table 3). The range of AGB was also wider for deciduous stands than for conifer stands (Table 3).

3.2. AGB and biomass density models

Using the tree biomass data and crown surface area calculated from r and b, new tree-biomass allometric equations were fit based on the observed linear relationship for both pine and aspen (Fig. 3). The crown SA data were related to tree biomass with a coefficient of determination (r^2) = 0.63 and root mean square error (RMSE) = 32.7 t/ha for 350 pine trees and an r^2 = 0.52 and RMSE = 69.8 t/ha for 350 aspen trees (Table 4). The RMSE values observed in these new crown SA models were higher than the RMSE reported for the same species based on dbh models (Case & Hall, 2008) or height and dbh models (Singh, 1982), however, the crown SA models were most appropriate for use with the output from the MFM-GOMS inversion due to the accurate b and r predictions.

3.3. Forest stand structure estimates from MFM inversion

Estimates of density obtained through MFM inversion were most accurate when the refined LUTs bounded by field observations and a smaller discrete increment through the structural parameter range were used (Table 2). Using these refined LUTs, average prediction error determined by absolute RMSE for density estimates was 590 stems/ha for pine plots and 310 stems/ha for aspen dominant plots. For the refined LUTs, the relative absolute error was 40% for pine and 27% for aspen. Although no comparable studies of AGB in mountainous areas exist for the range of terrain, density and tree species encountered here, we note that Wu and Strahler (1994) predicted stem density for nine lower-density conifer dominant stands over less variable terrain at 18% relative absolute error. The average prediction error for density estimates obtained from the general LUT, created using general structural inputs, was 1050 stems/ha for pine plots and 530 stems/ha for aspen. The aspen estimate error was similar in magnitude to the precision (discrete increment size) of density within the LUTs used for retrieval. This was expected since it was unlikely that the minimum average error would surpass the precision or increment size of the LUTs used in the estimation technique. Pine estimate error, however, was approximately double the increment size indicating that the precision of the LUT was not the limiting factor on the minimum average error in that case.

Table 4
Regression parameters, predictive strength (r^2) and standard error (S.E.) for crown surface area vs. calculated individual tree biomass for lodgepole pine and trembling aspen. p-value < 0.05.

	n	b_0	b_1	r^2	S.E.
Lodgepole pine	350	21.000	2.337	0.63	32.7 t/ha
Trembling Aspen	350	17.121	4.388	0.52	69.8 t/ha

Average prediction error for conifer horizontal crown radius (r) and vertical crown radius (b) was 0.4 m and 0.8 m RMSE respectively using the refined LUTs. Using the general LUTs, prediction error increased to 1.1 m for r and 1.2 m for b. Prediction error for deciduous r and b was 0.4 and 0.9 m RMSE respectively using the refined LUTs and 0.9 m and 1.0 m RMSE using the general LUTs. Thus, LUTs using *a priori* knowledge of field conditions and smaller increment sizes were more effective for predicting crown structure and reducing input error in subsequent biomass modeling. This relationship between parameter range and precision is at the foundation of the MFM full-blind processing method (Peddle, Boon, et al., in press) that uses general LUT ranges and coarse increments as the initial conditions in an optimization procedure that iteratively determines refined LUT ranges and increments automatically, thus removing the requirement for user-specified input range from ground data or other sources. This capability thus has implications for future regional scale MFM biomass retrievals.

3.4. Mapping forest biomass density from MFM inversion

3.4.1. Overall biomass results

Results for all plots are shown in Table 5 and summarized in Fig. 4. MFM had the lowest error (31.7 t/ha) of the three methods (SMA: 32.6 t/ha; NDVI: 34.7 t/ha). MFM output was also more similar to field values in terms of range (field: 67–243 t/ha; MFM: 79–249 t/ha) compared with SMA (134–191 t/ha) and NDVI (130–173 t/ha), and absolute range (field: 176 t/ha; MFM: 170 t/ha; SMA: 57 t/ha; NDVI: 43 t/ha). Mean values were all similar to the field, however, for standard deviation (SD), the only method similar to the field SD (38.2 t/ha) was MFM (SD: 41.7 t/ha), whereas SMA was 11.5 t/ha and NDVI 8.3 t/ha. This immediately indicates that SMA and NDVI have a considerably more narrow breadth of biomass output (see Figs. 5 and 6) and may be limited in this regard, yet MFM provided a more comprehensive range of biomass density for most of those values. In terms of high correspondence, 16 of the 36 validation plots had differences <20 t/ha using MFM (SMA: 13; NDVI: 11). MFM

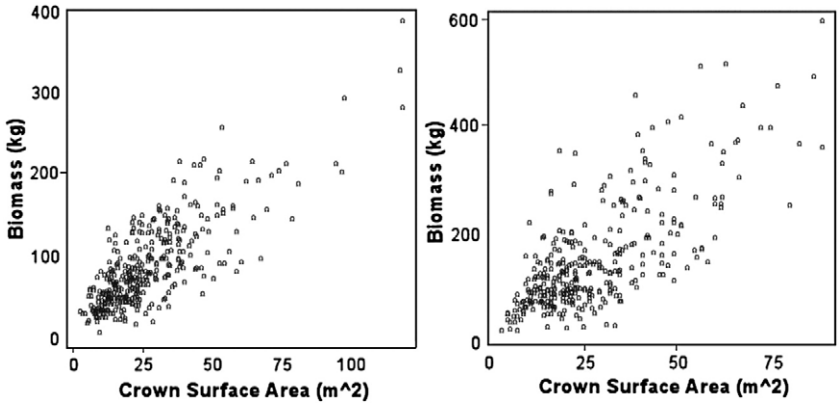

Fig. 3. Scatterplot of crown surface area and calculated individual tree biomass. Left: lodgepole pine. Right: trembling aspen.

Table 5
Biomass results for all deciduous and conifer plots ($n=36$) showing field data and estimates from NDVI, SMA and MFM. Result subsets shown for the 25 field plots that were within 1 standard deviation (<1 SD) of the overall biomass mean from all plots, and for the remaining 11 plots (>1 SD) to assess results over the full biomass range. All results in tonnes/hectare (t/ha).

All plots	*n* (plots)	Biomass avg	StDev	Min	Max	Range
Field	36	150.1	38.2	67	243	176
NDVI	36	156.1	8.3	130	173	43
Error (all plots)	36	34.7	27.1	4	107	103
Error (plots<1 SD)	25	20.2	13.0	4	49	45
Error (plots>1 SD)	11	67.5	21.4	42	107	65
SMA	36	149.5	11.5	134	191	57
Error (all plots)	36	32.6	25.1	0	102	102
Error (plots<1 SD)	25	20.0	12.8	0	44	44
Error (plots>1 SD)	11	65.5	18.5	46	102	56
MFM	36	153.2	41.7	79	249	170
Error (all plots)	36	31.7	28.4	0	97	97
Error (plots<1 SD)	25	29.0	24.6	0	97	97
Error (plots>1 SD)	11	37.9	36.3	0	93	93

results also had a greater consistency and lower overall error magnitude across a greater range of biomass field values when the field data set was assessed by SD categories. Higher error was found with SMA (65.5 t/ha) and NDVI (67.5 t/ha) compared with MFM (37.9 t/ha) for the 11 field plots beyond 1 SD of the field biomass mean, with much smaller differences (<10 t/ha) between MFM and the other methods for plots within 1 SD.

3.4.2. Conifer results

For conifer plots (Table 6 and Fig. 7), the accuracies for all methods were within 30 t/ha (MFM: 23.0 t/ha; SMA: 27.9 t/ha; NDVI: 29.7 t/ha). Although direct comparisons with other studies elsewhere cannot be made definitively, we note that this level of error is comparable to that reported by Hall et al. (2006) for a boreal conifer study (37.6 t/ha), and less accurate than the 20 t/ha difference reported by Hall et al. (1995) and the 18 t/ha in a mixed forest application reported by Peddle, Luther, et al. (2003), all of which were not in mountainous terrain.

Error levels for a minority of plots were considerably higher than average in both conifer and deciduous validaton sets. In particular, errors for three of the lodgepole pine validation plots were consistently high (>60 t/ha) regardless of method. The majority of the remaining lodgepole pine validation plots had error values less than 40 t/ha. The maximum difference between estimated and measured biomass from all methods ranged from 75–81 t/ha, with minimum error 0 t/ha. The overall error was thus affected by a few plots with error levels considerably larger than the majority. Of the 21 conifer validation plots, 13 had a difference of <20 t/ha using MFM (SMA: 9; NDVI 6), and 16 had a difference of <40 t/ha (SMA: 16; NDVI 15).

3.4.3. Deciduous results

There was less distinction amongst the three methods for deciduous biomass results (Table 7 and Fig. 8) compared to conifer plots. Overall, error for each of the three methods was within 4.5 t/ha. The average difference for deciduous using MFM was 43.8 t/ha, more than both NDVI (41.7 t/ha) and SMA (39.3 t/ha), and in all cases the biomass error was more than 10 t/ha greater than the corresponding conifer result by method. There were also plots within the deciduous validation set where the difference between measured and estimated values was considerably larger than the average. The maximum differences for all methods ranged from 97 to 107 t/ha, with minimum differences <4 t/ha. Using MFM, 3 of the 15 validation plots had

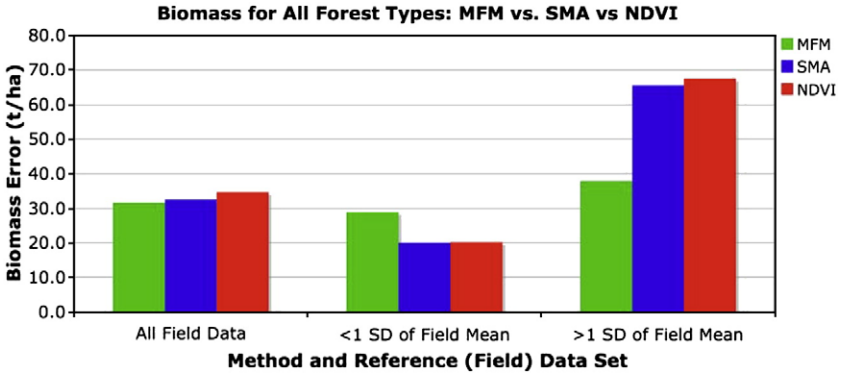

Fig. 4. Comparison of biomass estimation error for all conifer and deciduous plots from MFM, SMA and NDVI. Results shown for all plots ($n=36$), plots within 1 standard deviation (<1 SD) of the biomass plot mean ($n=25$), and plots outside 1 SD ($n=11$).

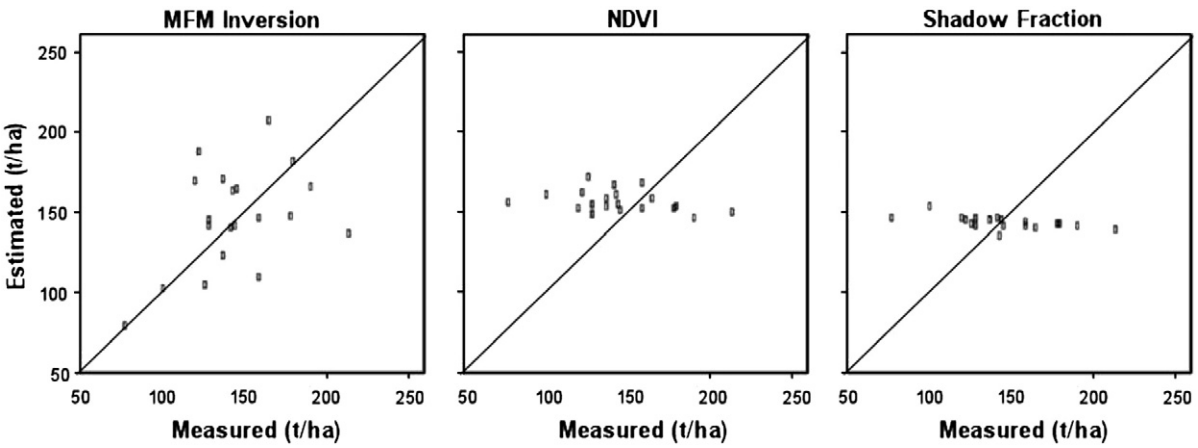

Fig. 5. Conifer biomass estimated using (L-R): MFM inversion, NDVI, and SMA shadow fraction. Results plotted against field-derived biomass validation data.

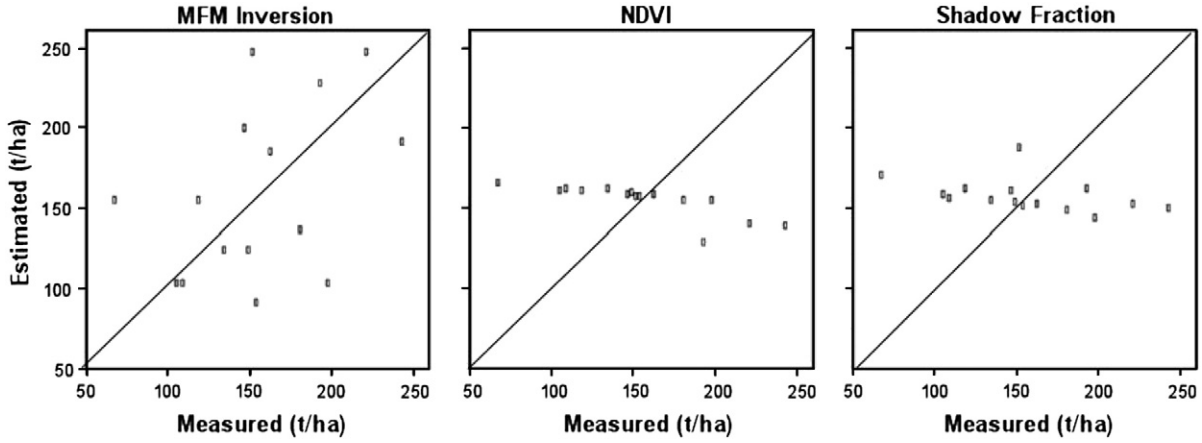

Fig. 6. Deciduous biomass estimated using (L-R): MFM inversion, NDVI, and SMA shadow fraction. Results plotted against field-derived biomass validation data.

Table 6
Biomass results (t/ha) for conifer plots ($n=21$) showing field data and estimates from NDVI, SMA and MFM. Result subsets shown for the 17 conifer plots that were within 1 standard deviation (<1 SD) of the overall biomass mean from all conifer plots, and for the remaining 4 conifer plots (>1 SD) to assess results over the full conifer biomass range.

Conifer	*n* (plots)	Biomass avg	StDev	Min	Max	Range
Field	21	141.0	34.0	73	213	140
NDVI	21	157.0	6.5	148	173	25
Error (all plots)	21	29.7	20.5	5	81	76
Error (plots<1 SD)	17	22.2	12.6	5	49	44
Error (plots>1 SD)	4	61.8	16.0	42	81	39
SMA	21	142.3	3.8	134	153	19
Error (all plots)	21	27.9	20.5	0	76	76
Error (plots<1 SD)	17	20.1	12.7	0	40	40
Error (plots>1 SD)	4	60.8	12.1	50	76	26
MFM	21	146.0	30.6	79	208	129
Error (all plots)	21	23.0	22.4	0	75	75
Error (plots<1 SD)	17	22.3	20.1	0	66	66
Error (plots>1 SD)	4	26.3	34.2	2	75	73

differences <20 t/ha (SMA: 4; NDVI: 5) and 8 had differences <40 t/ha (SMA: 8; NDVI: 7).

As with the conifer results, there were considerable differences in MFM performance vs. SMA and NDVI across the range of biomass values. MFM error was relatively consistent for all biomass values, whereas SMA and NDVI errors were much higher for almost half (7 of 15) of the plots with biomass values greater than 1 SD from the biomass field mean. In those cases, SMA and NDVI errors were between 68 and 71 t/ha, whereas MFM error was 44.6 t/ha. Values closer to the mean were considerably more accurate using SMA and NDVI in those cases, however, given the narrow range of these values for all plots (Table 7), it is difficult to confirm a true discriminatory capability beyond the clustering of values around the mean, some of which correspond. Regarding direction of error, there was no observed trend in error (e.g. overestimation, underestimation) in either the conifer or deciduous results (note: the absolute value of differences was used in all summary statistics of errors reported).

3.4.4. Biomass mapping

MFM was chosen for mapping AGB for the study area (Fig. 9) based on the superior biomass results obtained compared to SMA and NDVI, and also owing to the more direct, physically-based biophysical structural output that required application of only the established crown SA to biomass relationship to provide biomass output, unlike both SMA and NDVI which would require development of empirical equations within a statistical model for biomass. MFM AGB results were aggregated into four classes for mapping purposes. The spatial patterns of biomass density included, as expected, low values near roads, trails, cut-lines and cut-blocks, with higher biomass density values found primarily on north-northwest facing slopes and in high density lodgepole pine stands. Pixels for which no MFM structural solutions were possible occurred when there was no match between the image pixel and LUT values after all solution set processing was applied (Soenen et al., 2009). These pixels were assigned to a "no solution" structural class that was then propagated directly through to the biomass map as a mask (areas mapped as black in Fig. 9). This corresponded to areas including rivers, roads, rocky slopes and mountain summits, as well as Barrier Lake, however, the algorithm also masked areas of deep topographic shadowing. This erroneous masking, while not significant in extent, would have some effect on

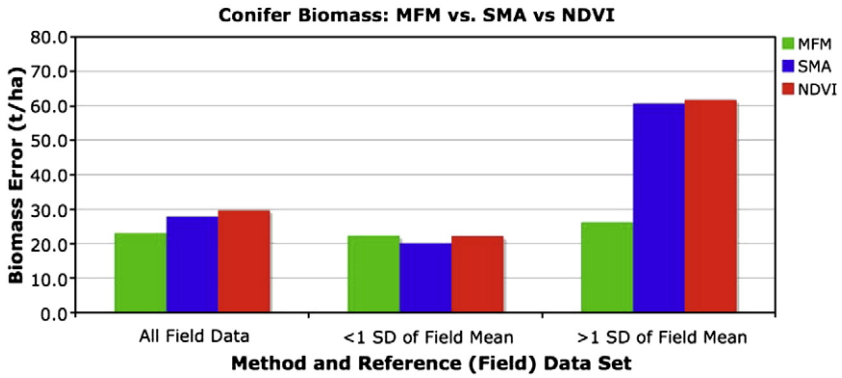

Fig. 7. Comparison of biomass estimation error for conifer plots from MFM, SMA and NDVI. Results shown for all conifer plots ($n=21$), plots within 1 standard deviation (<1 SD) of conifer biomass plot mean ($n=17$), and plots outside 1 SD ($n=4$).

Table 7
Biomass results (t/ha) for deciduous plots ($n=15$) showing field data and estimates from NDVI, SMA and MFM. Result subsets shown for the 8 deciduous plots that were within 1 standard deviation (<1 SD) of the overall biomass mean from all deciduous plots, and for the remaining 7 deciduous plots (>1 SD) to assess results over the full deciduous biomass range.

Deciduous	*n* (plots)	Biomass avg	StDev	Min	Max	Range
Field	15	155.0	46.0	67	243	176
NDVI	15	154.7	10.4	130	167	37
Error (all plots)	15	41.7	33.9	4	107	103
Error (plots<1 SD)	8	16.1	13.6	4	41	37
Error (plots>1 SD)	7	70.9	24.5	43	107	64
SMA	15	159.7	10.9	145	191	46
Error (all plots)	15	39.3	30.0	1	102	101
Error (plots<1 SD)	8	19.8	13.7	1	44	43
Error (plots>1 SD)	7	68.7	22.2	46	102	56
MFM	15	163.2	53.2	92	249	157
Error (all plots)	15	43.8	32.1	0	97	97
Error (plots<1 SD)	8	43.1	28.5	4	97	93
Error (plots>1 SD)	7	44.6	38.3	0	93	93

any subsequent biomass accounting and would likely be best addressed using macro-level terrain processing that was not considered here.

4. Discussion

The MFM inversion method for biomass density has advanced the MFM biophysical parameter estimation methodology by extending the capabilities toward prediction of second-order forest stand attributes that cannot be directly derived from satellite imagery. The results showed that the MFM method was suitable for making estimates of forest stand biomass density from multispectral image data, and the level of accuracy surpassed other empirical methods (SMA and NDVI). In mountainous terrain, the ability of MFM to incorporate terrain variability directly in the analysis (Soenen et al., 2008) meant that a separate topographic correction was not required. This is an important consideration as the influence of terrain on biomass estimation can be significant. This study provided a unique test-bed in this regard as the SPOT image data set had previously been subjected to extensive topographic corrections from various methods, from which the best non-MFM correction was available to this study using the SCS+C approach (Soenen et al., 2005). The direct handling of topography in MFM-GOMS is therefore part of the advantage of MFM in comparison with other methods. Furthermore, the MFM inversion method has several other key advantages such as use of more refined parameter classes with flexible class ranges and

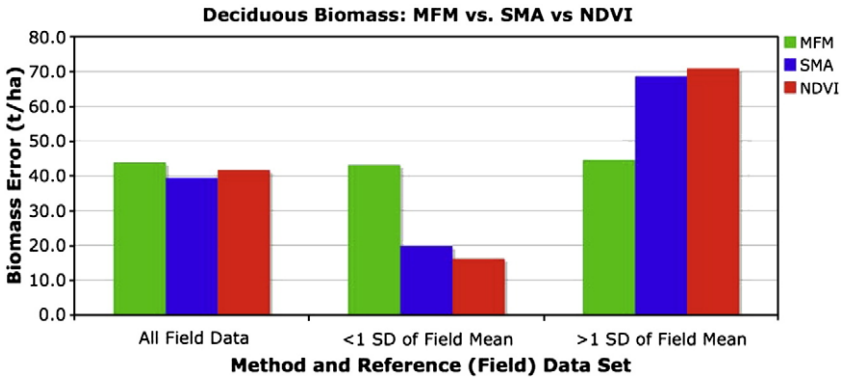

Fig. 8. Comparison of biomass estimation error for deciduous plots from MFM, SMA and NDVI. Results shown for all deciduous plots ($n=15$), plots within 1 standard deviation (<1 SD) of conifer biomass plot mean ($n=8$), and plots outside 1 SD ($n=7$).

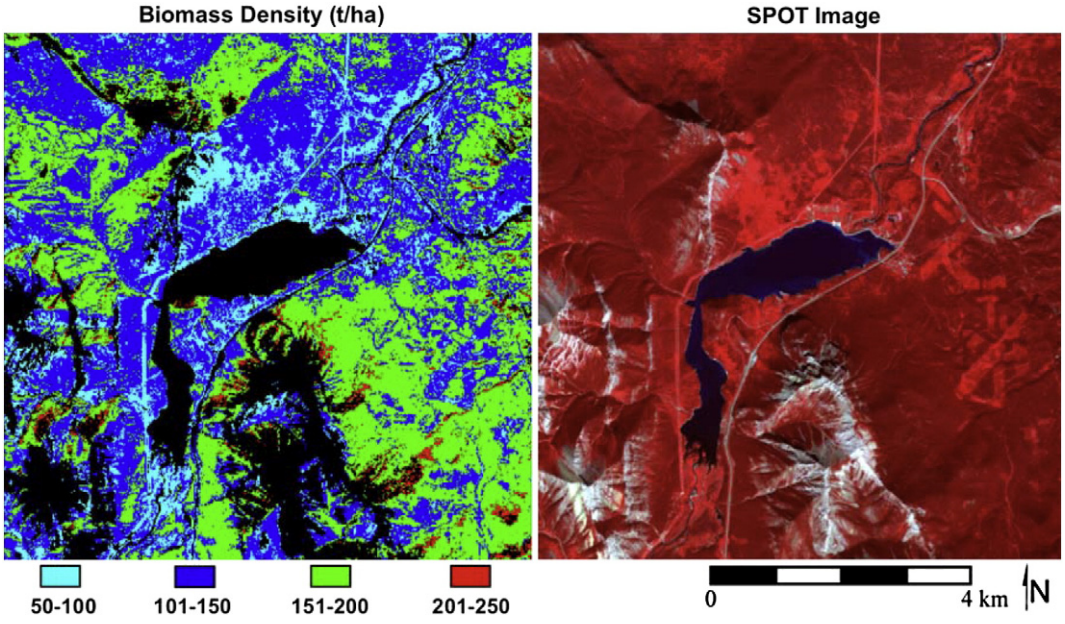

Fig. 9. Right: SPOT image (bands 3,2,1). Left: map of forest biomass density from MFM inversion, with results aggregated to 50 t/ha classes (black shows areas with no inversion results such as water, roads, bare rock, mountain summits etc.).

increments, the explicit physical parameterisation of sun-canopy-sensor geometry as well as forest stand attributes, the suitability to multi-image studies (different seasons and solar/view geometries are handled explicitly), and, perhaps most importantly, the ability to function fully with minimal or no field or *a priori* information (Peddle et al., 2007; Peddle, Boon, et al., in press).

With the canopy reflectance model inversion procedure, it is possible to operate with little or no field data to obtain forest structural outputs. If used to derive second-order parameters such as biomass, the physical relationship between first-order canopy variables (i.e. direct MFM output) and the parameter of interest (e.g. biomass) must be known or derived. Otherwise, general allometric relationships and biomass prediction equations could be used. To construct an empirical model, linear regression methods would require a spatially representative sample of the structural parameter of interest be acquired from the field. For large areas, particularly those that include remote, inaccessible terrain (Turner et al., 2004), the required resources are likely excessive and impractical, yet the increased variation for a given parameter makes a larger sample size essential for valid statistical testing. Alternatively, MFM can be run in partial or full-blind mode (Peddle, Boon, et al., in press) in which no *a priori* field or other information is required, and the method instead derives the necessary inputs automatically using a multi-stage optimisation procedure.

In regular MFM-mode (as used in this study), the minimum requirement for operation of the canopy reflectance model inversion method is spectral information for the primary overstory species, understory background, and shadowed vegetation. These spectral signatures can be measured in the field, extracted directly from the imagery, obtained from spectral libraries, or modeled, with hybrid approaches also feasible (e.g. Peddle et al., 1999). If, however, spectral signatures for endmembers are not available, MFM can determine these inputs internally based on partial or full-blind MFM procedures (Peddle, Boon, et al., in press), progressively increasing the precision of spectral ranges, similar to any other parameter. It should also be noted that, when *a priori* structural or other information is available, there are no constraints imposed, and even general structural information can increase estimation accuracy by bounding input ranges within the canopy reflectance model inversion method. This also results in faster computing times.

The minimal field data requirements of the MFM inversion procedure also have forest management implications since it is possible to characterize and map large swaths of forested area with limited field measurements. The MFM method is also scalable to coarser resolution data that allows larger areas of interest to be considered and may provide information about spatial distribution of AGB and how it relates to topography and forest stand characteristics.

In terms of biomass estimation (Tables 5–7), although subsets of results by terrain (slope, aspect), density and other properties was not explored directly in this paper, the canopy reflectance model based method appeared to provide superior results across a greater range of forest stand types and terrain conditions given the diversity of plots analysed. Additionally, the capability for biomass estimation was considerably different across the range of biomass validation values. Results indicated that SMA and NDVI had less discriminatory power across the full range of biomass values compared to MFM, a finding that has important implications when contemplating these various methods for larger area, regional scale applications.

Within the study, any unknown error introduced through discrepancies in tree measurements and inherent error within the dbh-based biomass model is likely to have propagated through to the MFM inversion estimates. While determining the source and extent of this error is beyond the scope of this study, it is important to acknowledge the existence of these potential errors that are external to the MFM modeling domain.

5. Conclusions

A new method was presented for estimating forest biomass which extends the capabilities of the existing MFM canopy reflectance model inversion toward deriving second-order parameters that cannot be directly estimated from satellite imagery. The method used indirect look-up table based canopy reflectance model inversion to obtain estimates of canopy dimensions and stand density. These first-order parameters were then related to biomass through empirical modeling. The MFM approach provided improved biomass density estimates compared to empirical NDVI and SMA methods, and offered considerable further advantages in terms of flexibility, reduced field requirements, suitability for larger areas involving multi-image/multi-temporal/multi-sensor data, and robustness of processing and analysis. The results also showed that MFM was suitable for a greater range of biomass densities compared to the other methods. Conceptually, the approach developed here provides flexibility and potential within a powerful and mature canopy reflectance model inversion context for deriving detailed biophysical information.

Acknowledgments

This research was supported in part by grants to Dr. Peddle and collaboration from the Natural Sciences and Engineering Research Council of Canada (NSERC), Alberta Ingenuity Centre for Water Research (AICWR), Prairie Adaptation Research Collaborative (PARC), Natural Resources Canada, NASA Goddard Space Flight Centre/University of Maryland, Alberta Research Excellence Program, Center for Remote Sensing, Boston University (GOMS model), and the University of Lethbridge. Computing resources were provided through the Western Canada Research Grid (West-Grid NETERA c3.ca). SPOT imagery was acquired from Iunctus Geomatics Corporation and the Alberta Terrestrial Imaging Centre (ATIC), both of Lethbridge Alberta. We are grateful to Sam Lieff, Adam Minke, and Kristin Yaehne for field assistance and the staff at the Kananaskis Field Stations for logistical support in the field.

References

Archibald, J. H., Klappstein, G. D., & Corns, I. G. W. (1996). *Field guide to ecosites of southwestern Alberta*. Vancouver, B.C: UBC Press Special Report 8.

ASD. (1998). *Fieldspec FR user's guide*.Boulder, CO: Analytical Spectral Devices Inc. 47 pp.

AVI (1991). *Alberta Vegetation Inventory Standards Manual Version 2.1*. Edmonton, AB: Alberta Environmental Protection, Resource Data Division, Data Acquisition Branch.

Bannari, A., Morin, D., Bonn, F., & Huete, A. R. (1995). A review of vegetation indices. *Remote Sensing Reviews*, *13*, 95—120.

Baskerville, G. L. (1972). Use of logarithmic regression in estimation of plant biomass. *Canadian Journal of Forestry*, *2*, 49—53.

Brown, S. (2002). Measuring carbon in forests: Current status and future challenges. *Environmental Pollution*, *116*, 363—372.

Case, B. S., & Hall, R. J. (2008). Assessing prediction errors of generalized tree biomass and volume equations for the boreal forest region of West-Central Canada. *Canadian Journal of Forest Research*, *38*, 878—889.

Chen, J. M. (1996). Evaluation of vegetation indices and a modified simple ratio for boreal applications. *Canadian Journal of Remote Sensing*, *22*(3), 229—242.

Chen, J. M., Li, X., Nilson, T., & Strahler, A. H. (2000). Recent advances in geometrical optical modelling and its applications. *Remote Sensing Reviews*, *18*, 227—262.

Cihlar, J., Denning, S., Ahern, F., Anno, O., Belward, A., Bretherton, F., et al. (2002). Initiative to quantify terrestrial carbon sources and sinks. *EOS. Transactions of the American Geophysical Union*, *83*(1), 6—7.

Cihlar, J., Guindon, B., Beaubien, J., Latifovic, R., Peddle, D., Wulder, M., et al. (2003). From need to product: A methodology for completing a land cover map of Canada using Landsat imagery.*Canadian Journal of Remote Sensing*, *29*(2), 171—186 Special Issue on Landsat-7.

Cohen, W. B., Maiersperger, T. K., Spies, T. A., & Oetter, D. R. (2001). Modeling forest cover attributes as continuous variables in a regional context with Thematic Mapper data. *International Journal of Remote Sensing*, *22*, 2279—2310.

Coops, N. C., White, J. D., & Scott, N. A. (2004). Effect of forest fragmentation on broad scale estimates of forest biomass accumulation. *International Journal of Remote Sensing*, *20*(4), 819—838.

De Jong, S. M., Pebesma, E. J., & Lacaze, B. (2003). Above-ground biomass assessment of mediterranean forests using airborne imaging spectrometry: The DAIS Peyne Experiment. *International Journal of Remote Sensing*, *24*(7), 1505—1520.

Elvidge, C. D., & Lyon, R. J. P. (1985). Influence of rock–soil spectral variation on the assessment of green biomass. *Remote Sensing of Environment*, *17*, 265—279.

ENVI. (2005). *ENVI/IDL image analysis system — User manual*. Boulder Colorado, USA: ITT Visual Information Solutions.

Foody, G. M., Boyd, D. S., & Cutler, M. E. J. (2003). Predictive relations of tropical forest biomass from Landsat TM data and their transferability between regions. *Remote Sensing of Environment*, *85*(4), 463—474.

Fournier, R. A., Luther, J. E., Guindon, L., Lambert, M. C., Piercey, D., Hall, R. J., et al. (2003). Mapping aboveground tree biomass at the stand level from inventory information: Test cases in Newfoundland and Quebec. *Canadian Journal of Forest Research*, *33*, 1846—1863.

Franklin, J., Davis, F. W., & Lefebvre, P. (1991). Thematic mapper analysis of tree cover in semiarid woodlands using a model of canopy shadowing. *Remote Sensing of Environment*, *36*, 189—202.

Franklin, S. E., Hall, R. J., Smith, L., & Gerylo, G. R. (2003). Discrimination of conifer height, age, and crown closure classes using Landsat-5 TM imagery in the Canadian Northwest territories. *International Journal of Remote Sensing*, *24*(9), 1823—1834.

Gamon, J. A., Huemmrich, K. F., Peddle, D. R., Chen, J., Fuentes, D., Hall, F. G., et al. (2004). Remote sensing in BOREAS: Lessons learned.*Remote Sensing of Environment*, *89*(2), 139—162 BOREAS Special Issue.

Gemmell, F. (1995). Effects of forest cover, terrain, and scale on timber volume estimation with thematic mapper data in a rocky mountain site. *Remote Sensing of Environment*, *51*, 291—305.

Gemmell, F. (1998). An investigation of terrain effects on the inversion of a forest reflectance model. *Remote Sensing of Environment*, *65*, 155—168.

Gerylo, G. R., Hall, R. J., Franklin, S. E., & Smith, L. (2002). Empirical relations between Landsat TM spectral response and forest stands near Fort Simpson, Northwest Territories, Canada. *Canadian Journal of Remote Sensing*, *28*, 68—79.

Green, R. (1979). *Sampling design and statistical methods for environmental biologists*. Toronto: Wiley Press.

Gu, D., & Gillespie, A. (1998). Topographic normalization of Landsat TM images of forests based on subpixel Sun-Canopy-Sensor geometry. *Remote Sensing of Environment*, *64*, 166—175.

Hall, F. G., Knapp, D. E., & Huemmrich, K. F. (1997). Physically based classification and satellite mapping of biophysical characteristics in the southern boreal forest. *Journal of Geophysical Research*, *102*(D24), 29567—29580.

Hall, F. G., Shimabukuro, Y. E., & Huemmerich, K. F. (1995). Remote sensing of forest biophysical structure using mixture decomposition and geometric reflectance models. *Ecological Applications*, *5*(4), 993—1013.

Hall, R. J., Skakun, R. S., Arsenault, E. J., & Case, B. S. (2006). Modeling forest stand structure attributes using Landsat ETM+ data: Application to mapping of aboveground biomass and stand volume. *Forest Ecology and Management*, *225*, 378—390.

Hame, T., Salli, A., Andersson, K., & Lohi, A. (1997). A new methodology for the estimation of biomass of conifer-dominated boreal forest using NOAA AVHRR data. *International Journal of Remote Sensing*, *18*(15), 3211—3243.

Hyyppä, J., Hyyppä, H., Inkinen, M., Engdahl, M., Linko, S., & Zhu, Y. -H. (2000). Accuracy comparison of various remote sensing data sources in the retrieval of forest stand attributes. *Forest Ecology and Management*, *128*, 109—120.

Jensen, J. R., & Hodgson, M. E. (1985). Remote sensing forest biomass: An evaluation using high resolution remote sensor data and loblolly pine plots. *Professional Geographer*, *37*(1), 46—56.

Kimes, D. S., Knyazikhin, Y., Privette, J., Abuelgasim, A., & Gao, F. (2000). Inversion methods for physically based models. *Remote Sensing Reviews*, *18*, 381—440.

Köhl, M., Magnussen, S., & Marchetti, M. (2006). *Sampling methods, remote sensing and GIS multiresource forest inventory*. New York: Springer-Verlag Press.

Kurz, W. A., & Apps, M. J. (1999). A 70-year retrospective analysis of carbon fluxes in the Canadian forest sector. *Ecological Applications*, *9*, 526—547.

Labrecque, S., Fournier, R. A., Luther, J. E., & Piercey, D. E. (2005). A comparison of four methods to map forest biomass from Landsat-TM and inventory data in Western Newfoundland. *Forest Ecological and Management*, *226*, 129—144.

Leblanc, S. G., & Chen, J. M. (2000). A windows graphic user interface (GUI) for the five-scale model for fast BRDF simulations. *Remote Sensing Reviews*, *19*, 293—305.

Leboeuf, A., Beaudoin, A., Fournier, R. A., Guindon, L., Luther, J. E., & Lambert, M. -C. (2005). A shadow fraction method to map biomass of Northern boreal black spruce forest using QuickBird imagery. *Remote Sensing of Environment*, *110*, 488—500.

Li, X., & Strahler, A. H. (1992). Geometric-optical bidirectional reflectance modeling of the discrete crown vegetation canopy: Effect of crown shape and mutual shadowing. *IEEE Transactions on Geoscience and Remote Sensing*, *30*, 276—292.

Lu, D. (2006). The potential and challenge of remote sensing-based biomass estimation. Review article. *International Journal of Remote Sensing*, *27*, 1297—1328.

Lu, D., Batistella, M., & Moran, E. (2005). Satellite estimation of aboveground biomass and impacts of forest stand structure. *Photogrammetric Engineering and Remote Sensing*, *71*(8), 967—974.

Luther, J. E., Fournier, R. A., Piercey, D. E., Guindon, L., & Hall, R. J. (2005). Biomass mapping using forest type and structure derived from Landsat TM imagery. *International Journal of Applied Earth Observation and Geoinformation*, *8*, 173—187.

Milton, E. J., Lawless, K., Roberts, A., & Franklin, S. E. (1997). The effect of unresolved scene elements on the spectral response of calibration targets: An example. *Canadian Journal of Remote Sensing*, *23*(3), 126—130.

Palacios-Orueta, A., Chuvieco, E., Parra, A., & Carmona-Moreno, C. (2005). Biomass burning emissions: A review of models using remote sensing data. *Environmental Monitoring and Assessment*, *104*, 189—209.

Parresol, B. R. (1999). Assessing tree and stand biomass: A review with examples and critical comparisons. *Forest Science*, *45*(4), 573—593.

Patenaude, G., Milne, R., & Dawson, T. P. (2005). Synthesis of remote sensing approaches for forest carbon estimation: Reporting to the Kyoto Protocol. *Environmental Science and Policy*, *8*, 161—178.

Peddle, D. R., Brunke, S. P., & Hall, F. G. (2001). A comparison of spectral mixture analysis and ten vegetation indices for estimating boreal forest biophysical information from airborne data. *Canadian Journal of Remote Sensing*, *27*(6), 627—635.

Peddle, D.R., Boon, S., Glover, A.P. & Hall, F.G., in press-a. Forest structure without ground data: Adaptive full-blind multiple forward-mode canopy reflectance model inversion with applications in a mountain pine beetle damaged forest. *International Journal of Remote Sensing*, *31*(8).

Peddle, D.R., Huemmrich, K.F., Hall, F.G., Masek, J.G., Soenen, S.A. & Jackson, C.D., in press-b. Applications of the BIOPHYS algorithm for physically-based vegetation continuous fields and forest disturbance. *IEEE Journal of Selected Topics in Applied Earth Observations and Remote Sensing* (IEEE J-STARS).

Peddle, D. R., & Johnson, R. L. (2000). Spectral mixture analysis of airborne remote sensing imagery for improved prediction of leaf area index in mountainous terrain, Kananaskis Alberta. *Canadian Journal of Remote Sensing*, *26*(3), 176—187.

Peddle, D. R., Johnson, R. L., Cihlar, J., & Latifovic, R. (2004). Large area forest classification and biophysical parameter estimation using the 5-scale canopy reflectance model in multiple-forward mode.*Remote Sensing of Environment*, *89*(2), 252—263 BOREAS Special Issue.

Peddle, D. R., Johnson, R. L., Cihlar, J., Leblanc, S. G., Chen, J. M., & Hall, F. G. (2007). Physically-based inversion modeling for unsupervised cluster labeling, independent forest classification and LAI estimation using MFM-5-scale. *Canadian Journal of Remote Sensing*, *33*(3), 214—225.

Peddle, D. R., Franklin, S. E., Johnson, R. L., Lavigne, M. A., & Wulder, M. A. (2003). Structural change detection in a disturbed conifer forest using a geometric optical reflectance model in multiple-forward mode. *IEEE Transactions on Geoscience and Remote Sensing*, *41*(1), 163—166.

Peddle, D. R., Luther, J. E., Pilger, N., & Piercey, D. (2003). Forest biomass estimation using a physically-based 3-D structural modeling approach for Landsat TM cluster labeling. *Proceedings, 25th Canadian Symposium on Remote Sensing, Montreal, PQ., Canada. Oct. 14–17, 2003Canadian Remote Sensing Society*, 12 pp. — on CD-ROM.

Peddle, D. R., White, H. P., Soffer, R. J., Miller, J. R., & LeDrew, E. F. (2001). Reflectance processing of remote sensing spectroradiometer data. *Computers & Geosciences*, *27*, 203—213.

Peddle, D. R., Hall, F. G., & LeDrew, E. F. (1999). Spectral mixture analysis and geometric optical reflectance modeling of boreal forest biophysical structure. *Remote Sensing of Environment*, *67*(3), 288—297.

Perry, C. R., Jr., & Lautenschlager, L. F. (1984). Functional equivalence of spectral vegetation indices. *Remote Sensing of Environment*, *14*, 169—182.

Rosenqvist, A., Milne, A., Lucas, R., Imhoff, M., & Dobson, C. (2003). A review of remote sensing technology in support of the Kyoto Protocol. *Environmental Science & Policy*, *6*, 441—455.

Roy, P. S., & Ravan, S. A. (1996). Biomass estimation using satellite remote sensing data — An investigation on possible approaches for natural forest. *Journal of Biosciences*, *21*(4), 535—561.

Rouse, J. W., Jr., Haas, R. H., Deering, D. W., & Schell, J. A. (1973). Monitoring the vernal advancement and retrogradation (greenwave effect) of natural vegetation. *NASA Goddard Space Flight Centre: GSFC Type II Report, Greenbelt, MD, USA. October 1973* Available at [verified August 28, 2009]: http://ntrs.nasa.gov/archive/nasa/casi.ntrs.nasa.gov/19740004927_1974004927.pdf

Scarth, P., & Phinn, S. (2000). Determining forest structural attributes using an inverted geometric-optical model in mixed eucalypt forests, Southeast Queensland, Australia. *Remote Sensing of Environment*, *71*, 141—157.

Schott, J. R., Salvaggio, C., & Volchok, W. J. (1988). Radiometric scene normalization using pseudoinvariant features. *Remote Sensing of Environment*, *26*, 1—16.

Seed, E. D., & King, D. J. (2003). Shadow brightness and shadow fraction relations with effective LAI: Importance of canopy closure and view angle in mixedwood boreal forest.*Canadian Journal of Remote Sensing*, *29*, 324—335 Special Issue on LAI.

Singh, T. (1982). Biomass equations for ten major tree species of the prairie provinces. *Canadian Forest Service, Northern Forest Research Centre, Edmonton, Alta. Information Report NOR-X-242*.

Smith, G. M., & Milton, E. J. (1999). The use of the empirical line method to calibrate remotely sensed data to reflectance. *International Journal of Remote Sensing*, *20*, 2653—2662.

Soenen, S. A., Peddle, D. R., Coburn, C. A., Hall, R. J., & Hall, F. G. (2009). Canopy reflectance model inversion in multiple forward mode: Forest structural information retrieval from solution set distributions. *Photogrammetric Engineering & Remote Sensing*, *75*(4), 361—374.

Soenen, S. A., Peddle, D. R., Coburn, C. A., Hall, R. J., & Hall, F. G. (2008). Improved topographic correction of forest image data using a 3-D canopy reflectance model in multiple forward mode. *International Journal of Remote Sensing*, *29*(4), 1007—1027. doi:10.1080/01431160701311333.

Soenen, S. A., Peddle, D. R., & Coburn, C. A. (2005). SCS+C: A modified sun-canopy-sensor topographic correction in forested terrain. *IEEE Transactions on Geoscience and Remote Sensing*, *43*(9), 2149—2160.

SPOT Image (2004). *SPOT sensor calibration, response functions and illumination geometry*. Toulouse, France: SPOT Image Corporation.

Thenkabail, P. S., Stucky, N., Griscom, B. W., Ashton, M. S., Diels, J., Van Der Meer, B., et al. (2004). Biomass estimations and carbon stock calculations in the oil palm plantations of African derived savannas using IKONOS imagery. *International Journal of Remote Sensing*, *25*(23), 5447—5472.

Thomas, V., Finch, D. A., McCaughey, J. H., Noland, T., Rich, L., & Treitz, P. M. (2006). Spatial modelling of the fraction of photosynthetically active radiation absorbed by a boreal mixedwood forest using a lidar-hyperspectral approach. *Agricultural and Forest Meteorology*, *140*, 287—307.

Treitz, P. M., & Rogan, J. (2004). Remote sensing for mapping and monitoring land-cover and land-use change — An introduction. In P. M. Treitz (Ed.), *Remote*

Sensing for Mapping Land Cover and Land Use ChangeProgress in Planning, vol. 61 (3). (pp. 269−279).

Turner, D. P., Ollinger, S. V., & Kimball, J. S. (2004). Integrating remote sensing and ecosystem process models for landscape- to regional-scale analysis of the carbon cycle. *BioScience*, *54*(6), 573−584.

van der Heijden, G. W. A. M., Clevers, J. G. P. W., & Schut, A. G. T. (2007). Combining close-range and remote sensing for local assessment of biophysical characteristics of arable land. *International Journal of Remote Sensing*, *28*(24), 5485−5502.

Weiss, M., Baret, F., Myneni, R. B., Pragnere, A., & Knyazikhin, Y. (2000). Investigation of a model inversion technique to estimate canopy biophysical variables from spectral and directional reflectance data. *Agronomie*, *20*, 3−22.

Woodcock, C. E., Collins, J. B., Jakabhazy, V. D., Li, X., Macomber, S. A., & Wu, Y. (1997). Inversion of the Li-Strahler canopy reflectance model for mapping forest structure. *IEEE Transactions on Geoscience and Remote Sensing*, *2*, 405−414.

Wu, Y., & Strahler, A. H. (1994). Remote estimation of crown size, stand density, and biomass on the Oregon transect. *Ecological Applications*, *4*(2), 299−312.

Wulder, M. A. (1998). Optical remote sensing techniques for the assessment of forest inventory and biophysical parameters. *Progress in Physical Geography*, *22*, 449−476.

Zheng, D., Rademacher, J., Chen, J., Crow, T., Bresee, M., Le Moine, J., et al. (2004). Estimating aboveground biomass using Landsat 7 ETM+ Data across a managed landscape in Northern Wisconsin, USA. *Remote Sensing of Environment*, *93*, 402−411.